Energy 84 (2015) 91–97

Contents lists available at ScienceDirect

Energy

journal homepage: www.elsevier.com/locate/energy

Current controller for a bidirectional boost input stage equipped with an *LCL* (inductance–capacitance–inductance) filter

Roberto Fantino, Claudio Busada, Jorge Solsona*

Instituto de Investigaciones en Ingeniería Eléctrica (IIIE) "Alfredo Desages" (UNS-CONICET), Departamento de Ingeniería Eléctrica y de Computadoras, Universidad Nacional del Sur (UNS), 8000 Bahía Blanca, Argentina

ARTICLE INFO

Article history:
Received 8 August 2014
Received in revised form
22 January 2015
Accepted 14 February 2015
Available online 25 March 2015

Keywords:
LCL (inductance–capacitance–inductance) filter
Active damping
Current control

ABSTRACT

A control strategy for a low resonance frequency *LCL* (inductance–capacitance–inductance) filter used in the input stage of dc–dc bidirectional boost converters is proposed. When compared with the classical L filter, an *LCL* filter allows to obtain a cheaper topology. However, with an *LCL* topology, damping is needed for guaranteeing the system stability. In this paper an active damping strategy is designed. The needed damping is achieved via a dynamic controller. The controller consists of a simple PI (proportional-integral) controller plus a linear filter added in series with the PI integrator term. The modified PI controller achieves the active damping of the *LCL* filter and allows to arbitrarily place the system closed-loop poles. The proposed strategy only requires measurement of the variable to be controlled, the source current. Simulation and experimental results validate the proposed controller and show its effectiveness.

© 2015 Elsevier Ltd. All rights reserved.

1. Introduction

In many renewable resource applications and dc distribution systems, dc–dc converters presenting a very low high-frequency ripple input current are needed [1–5]. In these applications, a bidirectional boost input stage equipped with an *L* filter is often included [6–11]. Many times, in order to attenuate the high frequency ripple appearing in the input current, interleaving converters are used [12–15]. Although, *LCL* (inductance–capacitance–inductance) filters are often used in grid connected inverters [16–21], it is unusual to find proposals where this kind of filters are used to reduce the high frequency ripple appearing in the dc–dc converter input current.

It is well-known that the presence of an *LCL* filter complicates the current controller design, because the filter presents a natural resonance frequency and increases the order of the dynamics. When the resonance frequency of the filter is high and it is placed far from the open-loop system unit gain frequency, it is possible to design the current controller by neglecting the dynamics introduced by the filter's capacitor [22]. Nevertheless, from the ripple reduction point of view, it is desirable to fix a resonance frequency as low as possible and to place it very below of the PWM (pulse-width modulation) frequency. In this way, the high frequency ripple attenuation provided by the *LCL* filter is much greater than that provided by the *L* filter. However, when the current controller is designed by the classic method based on the phase margin, the minimum value of the resonance frequency of the filter is limited below. It is because stability reasons, since when the resonance frequency is very low, the closed-loop system becomes unstable [23]. In Ref. [24], in order to ensure the stability of the closed-loop system, it is recommended to locate the resonance frequency four times above of the current controller bandwidth.

When the *LCL* filter is connected to a source with very low output impedance, it is required to damp the filter resonance. There are two ways to generate the needed damping. One of them uses passive methods, whereas the other one uses active methods. In high efficient systems, it is recommendable to avoid passive methods because these methods, based on dissipative elements, add losses to the system [21,25]. On the other hand, many times active damping methods include extra sensors for measuring either two currents or a current and a capacitor voltage [22,24,26–30]. The increase in the hardware complexity is the major disadvantage of these approaches.

Active damping can also be achieved without using additional sensors [31–33]. The strategy consists in filtering the voltage input to the PWM modulator by a linear filter. While this strategy can stabilize the system, to the best knowledge of the authors, there is no filter design method for attaining the system closed-loop poles assignation.

* Corresponding author. Tel.: +54 291 459 5101; fax: +54 291 459 5154.
E-mail addresses: zoomssc@hotmail.com (R. Fantino), cbusada@uns.edu.ar (C. Busada), jsolsona@uns.edu.ar (J. Solsona).

http://dx.doi.org/10.1016/j.energy.2015.02.045
0360-5442/© 2015 Elsevier Ltd. All rights reserved.

It must be remarked that few applications present an *LCL* scheme allowing to place all closed-loop poles of the system in an arbitrary way. To this end, a full state feedback is used in Ref. [34]. In order to implement this strategy three sensors are needed, since two filter currents and the capacitor voltage must be measured. In Ref. [35], a scheme based on virtual sensors is proposed. There, two states are measured and the remaining is obtained by using an observer.

Most of the applications found in the literature address to control the converter-side current of the filter, instead of the source-side current of the filter. This practice is explained by the fact that the feedback of the converter-side current itself introduces damping in the closed-loop system [28].

In this paper a new control scheme is proposed. The proposal consists in controlling the current drained to the source by a bidirectional boost converter connected to it through an *LCL* filter with low resonance frequency by using a modified PI controller. The modification consists in adding a linear network in series with the PI integral term. In this way, the modified PI damps the filter in an active way and allows to place all closed-loop poles of the system in an arbitrary way. In order to implement this controller, only the measurement of the current to be controlled is needed. Consequently, this controller can be implemented by using only one sensor, as shown in Ref. [36].

The rest of the paper is structured as follows. In Section 2, the proposed controller is introduced. In Section 3, a typical case of design is analyzed. Section 4 shows simulation and experimental results. Finally, in Section 5 conclusions are drawn.

2. Proposed controller

Fig. 1a shows a bidirectional boost input stage with an *LCL* filter. In the sequel, it will be assumed a source (v_p) with output resistance equal to zero. This assumption is included to consider the worst damping case. It is clear that a resistance value different from zero facilitates the damping because it is a dissipative element. It is possible to assume $v_p = 0$ to analyze the system behavior, since v_p is an external input. The transfer function between i_p and v_i, with $v_p = 0$, becomes:

$$H_F = \frac{I_p(s)}{V_i(s)} = -\frac{1}{L_1 L_2 C s(s^2 + \omega_0^2)} \tag{1}$$

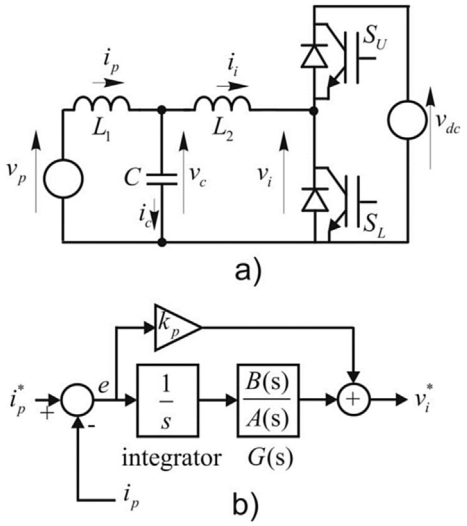

Fig. 1. Input stage with *LCL* filter (top). Modified PI controller (bottom).

where $I_p(s)$ and $V_i(s)$ represent the Laplace transforms of i_p and v_i respectively, and $\omega_0 = \sqrt{1/L_p C}$, with $L_p = L_1 L_2/(L_1 + L_2)$. In a practical application, it is needed to model the sampling process, and the delay introduced by the computation in the DSP (digital signal processor). Both effects can be modeled by using a first order relationship between the PWM modulator input reference (v_i^*) and the converter output voltage v_i [37]. This first order filter results

$$D_1 = V_i(s) \Big/ V_i^*(s) = \omega_c/(s + \omega_c) \tag{2}$$

where $V_i^*(s)$ and $V_i(s)$ represent the v_i^* and v_i Laplace transforms, respectively; $\omega_c = 1/1.5T_s$, and T_s stands for the sampling time. The phase introduced, in the control loop, by the transfer function (2) is shown in Fig. 2, together to the phase introduced by a pure delay equal to $T_p = 1.5T_s$, whose transfer function is given by $D(s) = e^{-sT_p}$ with $T_s = 10^{-4}$ ($f_s = 1/T_s = 10$ KHz). Note that, at high frequency, the delay introduced by the pure delay is greater than the delay introduced by the approximation. Consequently, when (2) is used for approximating the delay during a closed-loop controller design, the actual system phase margin will be worse than the predicted phase margin.

In the figure, it can be seen that the phase error introduced by the approximation is equal to 1.77 at 500 Hz $= f_s/20$, whereas the error is equal to 10.7 at 1 KHz $= f_s/10$. It is clear that in order to use the approximation, the bandwidth (f_{bw}) in closed-loop must be limited. In our case, if it is desired to damp the *LCL* filter resonance frequency placed at $f_0 = \omega_0/2\pi$, then the value of this frequency must be restricted to a frequency band where the approximation (2) is acceptable. A conservative bound is to choice f_0 and f_{bw} lesser than $f_s/10$. At this frequency, the introduced phase error is below of 10.7°. In such a case, the bandwidth duplicates the usual bandwidth. In Ref. [38], the approximation (2) is used for designing a discrete PI controller for an *L* filter, and it is recommended to use $f_{bw} < f_s/20$ for obtaining an acceptable response.

In order to put in context the role played by f_0 range, note that in Ref. [16], where active damping by capacitor voltage feedback is applied, is recommended to use $f_0 \approx f_s/3.4$. In our proposal, a resonance frequency f_0 very lower of that limit will be selected, such that the high frequency ripple presented in i_p will be notably reduced. In addition, in Ref. [39], where a PR (proportional-resonant, equivalent to a PI in a *dq* synchronous frame) regulator is analyzed, was concluded that it is not possible to stabilize the closed-loop by using i_p feedback when $f_0 < f_s/6$. For this reason,

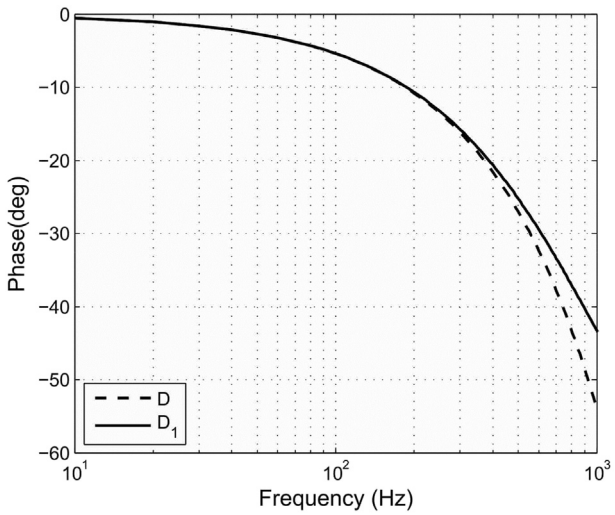

Fig. 2. Phase plot D (dashed line) and D_1 (full line), $T_s = 10^{-4}$.

there, the authors proposed to feedback the capacitor current i_c, which requires to add an additional current sensor. On the contrary, as explained below, in our proposal, additional sensors will not be needed to stabilize an *LCL* filter with low resonance frequency.

By using (2) in (1) results,

$$\frac{I_p(s)}{V_i^*(s)} = -\frac{c_0}{P(s)} = -\frac{c_0}{s(s^2+\omega_0^2)(s+\omega_c)} \tag{3}$$

where $c_0 = \omega_c/L_1L_2C$.

In order to control the *LCL* filter, a standard PI (many times, it is used for controlling an *L* filter), will be modified. A linear filter, whose transfer function is given by $G(s) = B(s)/A(s)$, is included in the PI integral term way, such as it is shown in Fig. 1b. The $G(s)$ order and relative degree must be three and zero, respectively. Then,

$$G(s) = \frac{B(s)}{A(s)} = \frac{b_3s^3 + b_2s^2 + b_1s + b_0}{s^3 + a_2s^2 + a_1s + a_0} \tag{4}$$

The system closed-loop transfer function, $H_{CL}(s) = I_p(s)/I_p^*(s)$ with $I_p^*(s)$ the Laplace transform of the current reference i_p^*, results

$$H_{CL}(s) = \underbrace{\frac{-c_0\left[sA(s)k_p + B(s)\right]}{sA(s)P(s) + c_0\left[sA(s)k_p + B(s)\right]}}_{D_{CL}(s)} \tag{5}$$

The closed-loop system has eight states. Four of them are needed to represent the system given by (3). The other four are provided by the PI controller -one state- and the linear network given by (4). Consequently, the degree of the polynomial $D_{CL}(s)$ -see (5)- is eight. The proposed controller structure allows to arbitrarily place the eight roots of $D_{CL}(s)$. To this end, it is sufficient to choice the eight constants (k_p, $a_{i=0,1,2}$ and $b_{i=0,1,2,3}$) in an adequate way. To verify it, let $a_j^*, j = 0, 1,\ldots,7$ be eight arbitrary constants, and assume that the constants k_p, a_i and b_i are selected according to,

$$a_2 = a_7^* - \omega_c \tag{6}$$

$$a_1 = a_6^* - \omega_0^2 - \omega_c a_2 \tag{7}$$

$$a_0 = a_5^* - \omega_0^2(\omega_c + a_2) - \omega_c a_1 \tag{8}$$

$$k_p = \left[a_4^* - \omega_0^2(a_2\omega_c + a_1) - \omega_c a_0\right]\Big/ c_0 \tag{9}$$

$$b_3 = \left[a_3^* - \omega_0^2(a_1\omega_c + a_0) - c_0k_pa_2\right]\Big/ c_0 \tag{10}$$

$$b_2 = \left[a_2^* - \omega_0^2 a_0\omega_c - c_0k_pa_1\right]\Big/ c_0 \tag{11}$$

$$b_1 = a_1^*/c_0 - k_pa_0 \tag{12}$$

$$b_0 = a_0^*/c_0. \tag{13}$$

By using the choice given by (6)–(13), it can be verified that

$$D_{CL}(s) = s^8 + \sum_{j=0}^{7} a_j^* s^j \tag{14}$$

In order to obtain (14), (6)–(13) are introduced into (3)–(5). Then, by suitably selecting the controller's parameters, it is possible to obtain an eight order polynomial $D_{CL}(s)$ with arbitrary coefficients. Thereby, the method for designing the controller results

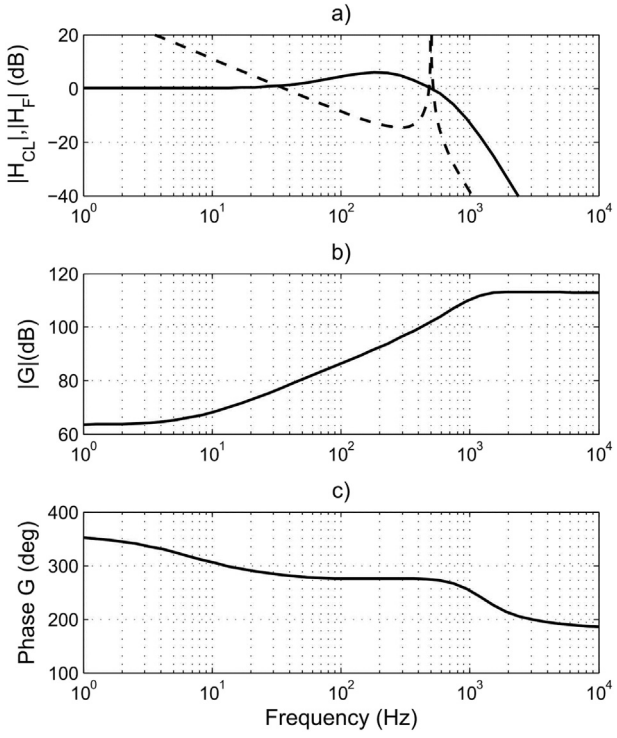

Fig. 3. a) Bode plot of the calculated H_F filter (dashed line) and closed-loop system H_{CL} (solid line). b) and c) $G(s)$ Modulus and phase, respectively.

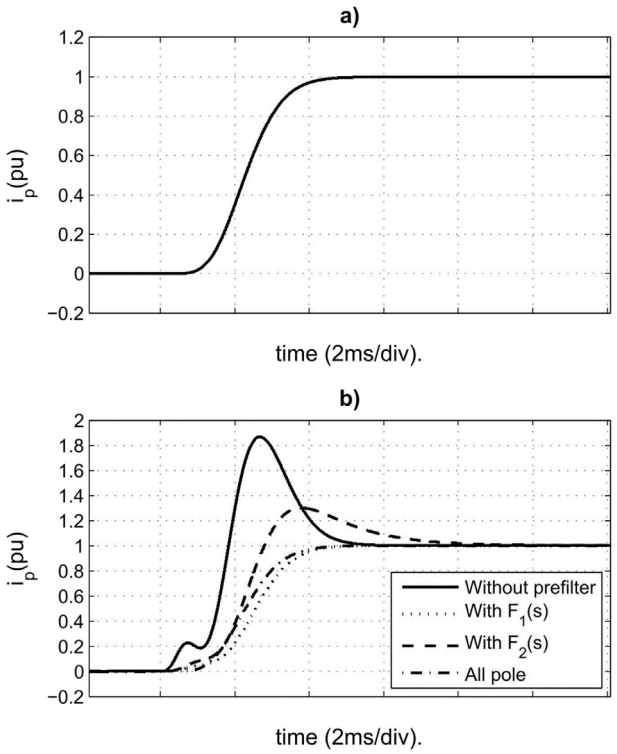

Fig. 4. Step time response a) $1/D_{CL}(s)$ system. b) Eq. (5) system.

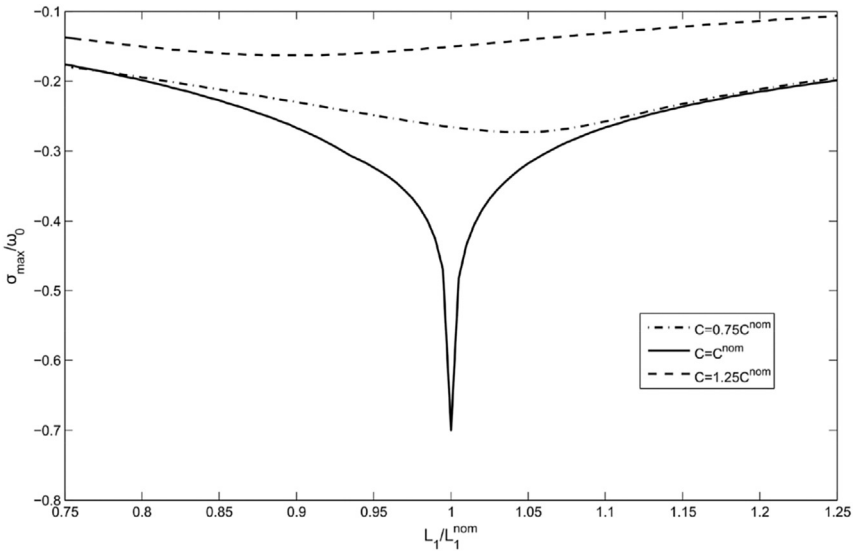

Fig. 5. σ_{max}/ω_0 for different values of L_1 and C.

simple. Once specified the desired positions of the closed-loop poles, the $a_j^*, j = 0, 1,\ldots,7$ values are calculated such that the roots of $D_{CL}(s)$ (see (14)) are at those positions. Then, from these values, the controller's parameters (k_p, $a_{i=0,1,2}$ and $b_{i=0,1,2,3}$) are obtained by using (6)–(13). In brief, the linear network described by (4), connected in series with the PI integral term, allows to actively damp the filter by arbitrarily assigning the system closed-loop poles. It must be noted that additional sensors are not needed to achieve it. Note that, due to design reasons, it is needed to use a structure such as that defined by (4). By using this structure, the closed-loop presents eight states (poles to be placed) and eight independent constants k_p, $a_{i=0,1,2}$ and $b_{i=0,1,2,3}$ can be selected to arbitrarily place the eight closed loop poles. If a transfer function $G_1(s)$ with degree two and relative degree zero, such as

$$G_1(s) = \frac{B_1(s)}{A_1(s)} = \frac{b_2 s^2 + b_1 s + b_0}{s^2 + a_1 s + a_0} \tag{15}$$

is selected, a seventh order closed-loop system results, while the controller only has six independent parameters to be designed. Consequently, this structure of $G_1(s)$ does not allows to arbitrarily place the seven closed-loop poles. Thus, it must be remarked that the transfer function given by (4) represents the transfer function having the minimum degree and allowing to place the closed-loop poles system in an arbitrary way.

The proposed method only allows to arbitrarily place the closed-loop poles, but it is not possible to assign the zeros, since they are defined by $A(s)$, $B(s)$ and k_p, according to (5). It is well known that in linear dynamical systems, the time response depends not only of

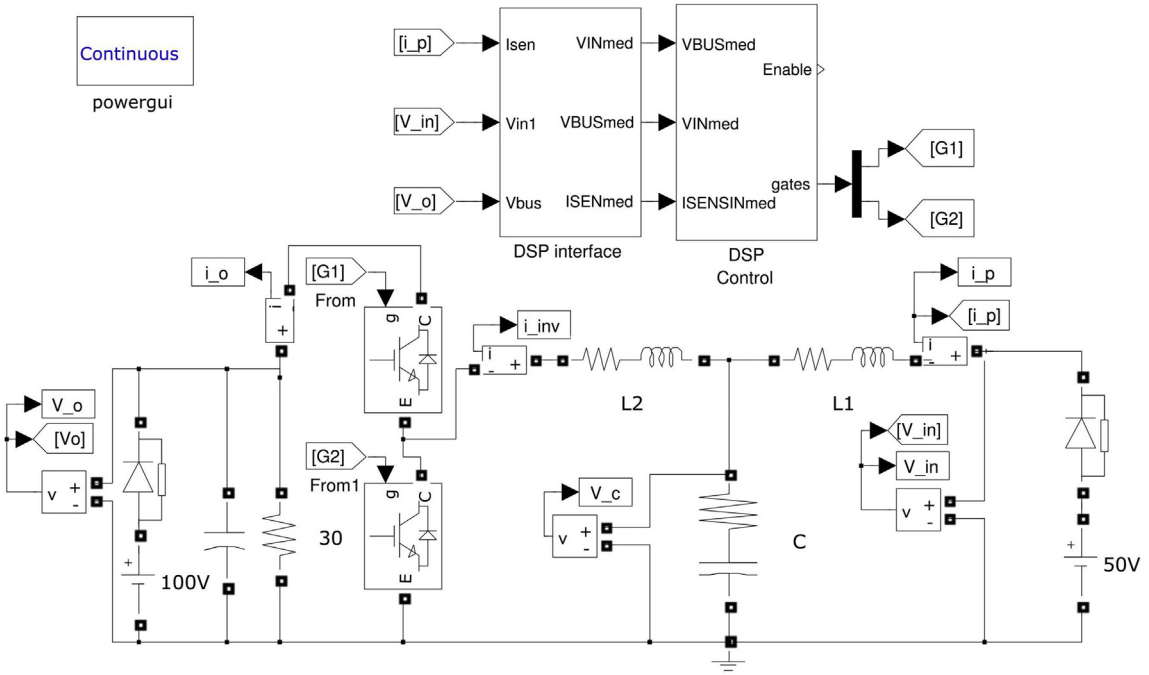

Fig. 6. Simulation diagram.

the poles position but also of the zeros position. A zero in the half left-hand plane, denoted by $(s/\omega_z + 1)$, where $\omega_z > 0$, introduces a term proportional to the reference input current (i_p^*) time derivative. This term tends to cause peaks in the time response. On the other hand, a zero in the half right-side hand plane (i.e. $\omega_z < 0$), introduces a term causing an inverse response. The peaks can be adjusted by canceling the zeros of the transfer function (5) placed in the half left-hand plane. This can be achieved by pre-filtering the reference i_p^*, by a filter with transfer function given by $F_1 = 1/Z(s)$, where $Z(s)$ roots coincide with the zeros to be canceled. However, generally it is not needed to cancel all zeros, it is enough to cancel the dominant zeros. The following section illustrates this issue.

3. Designing a typical case

The proposed controller behavior will be analyzed. It is assumed a sampling frequency $f_s = 10$ Khz($\omega_c = 1/1.5T_s = 6.66\ 10^3$rad/s), and an *LCL* filter with $L_1 = L_1^{nom} = 2.35$ mH, $L_2 = 2.1$ mH and $C = C^{nom} = 91$ μF($f_0 = \omega_0/2\pi = 501$ Hz). This filter was designed to obtain a resonance frequency lesser than ten times the sample frequency, i. e. $f_0 = f_s/19.96 < f_s/10$. This design follows recommendations presented in Ref. [24].

The controller parameters are calculated for obtaining the following closed-loop poles map:

- a complex poles pair at $0.7\omega_0(-1 \pm j)$
- six poles at $-\omega_0$

In order to design the controller, first the coefficients a_j^*, $j = 0$, 1,…7 of the polynomial (16) are computed. It is the denominator of the closed-loop transfer function defined in (5).

$$D_{CL}(s) = [s + 0.7\omega_0(1 + j)][s + 0.7\omega_0(1 - j)](s + \omega_0)^6 \qquad (16)$$

Then, by using these coefficients together with ω_0 and ω_c, the controller parameters k_p, $a_{i=0,1,2}$ and $b_{i=0,1,2,3}$ are calculated from (6)–(13).

Fig. 3a shows the modulus of the transfer function $H_F = I_p(s)/V_i(s)$ of the used *LCL* filter (dotted trace) (see (1)) and the modulus of the closed-loop transfer function defined by (5), H_{CL}. The H_{CL} −3 dB frequency is equal to 631 Hz ($f_{bw} = f_s/15.9$). Note that the filter resonance frequency, $f_0 = 501$ Hz, falls in the closed-loop system bandwidth. This confirms that the proposed method can be used for designing active damping when the resonance frequency of the filter is located in the bandwidth of the system to be controlled.

The main advantage of using a low resonance frequency is that, at the PWM frequency, a very small ripple value of the current drained from v_p is obtained. It must be noted that, by using *LCL* filters, it is possible to diminish the resonance frequency by increasing the filter capacitor value and by keeping the inductance values. However, when an *L* filter is used, the only way of reducing the PWM ripple is to increase the value of the inductance connected between the converter and the source.

Fig. 3b and c shows the $G(s)$ -see Eqn. (15)-, frequency response. It can be seen that at low frequencies this transfer function behaves as a constant. This constant represents the low frequency gain of the integrator term of the PI. At high frequencies, $G(s)$ also behaves as a constant gain, but it presents a negative sign (phase 180°), which implies a positive feedback. The loop stability is not affected because the unitary gain is below of these frequencies. At media frequencies, the gain increases 20 dB/dec.

Fig. 4b, full trace, shows the time response to a step signal in the ideal closed-loop system (5). The time response presents an overshoot equal to 87%. In many applications this overshoot is not tolerable. As explained in Section 2, the overshoot is originated by the presence of half left-hand plane zeros in the transfer function (5). A system having a complex pole at $0.7\omega_0(-1 \pm j)$ and six poles at $-\omega_0$, whose transfer function has not zeros, would allow to obtain an underdamped response. Fig. 4a shows the response of this system. The transfer function (5) has four zeros. For the designed controller, these zeros are at $s_1 = -387$, $s_2 = -6463$ (half left-hand plane), and $s_{3,4} = 1349 \pm 2304j$ (half right-hand plane). Note that, the distance from the origin to s_1 is smaller than the distance from s_2 to the origin, then s_1 is a dominant zero. It is possible to filtering i_p^* by using a filter whose transfer function is $F_1 = 1/(-s/s_1 + 1)$. In Fig. 4b the dotted line shows the system response when i_p^* has been filtered by F_1. For comparison, in Fig. 4b is included (see dash-dotted line) the response shown in Fig. 4a. It can be seen that the time response is almost the same. Many times, it is desirable to obtain an overshoot. This overshoot can be obtained by canceling the dominant zero in a partial way. The

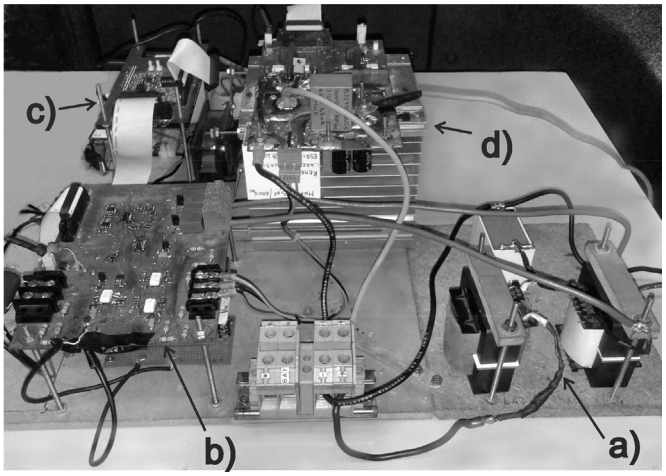

Fig. 7. Experimental set up. (a) *LCL* filter; (b) Sensors; (c) DSP and DSP interface; (d) Boost converter.

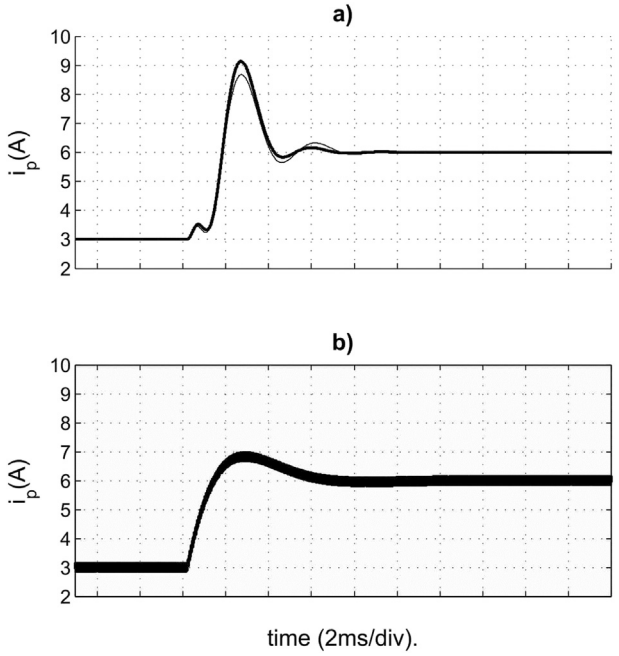

Fig. 8. Injected current i_p. a) *LCL* case. Thick trace: ideal case. Thin trace: L_1, L_2 and *C* with ESR. b) *L* case (scale 1A/div).

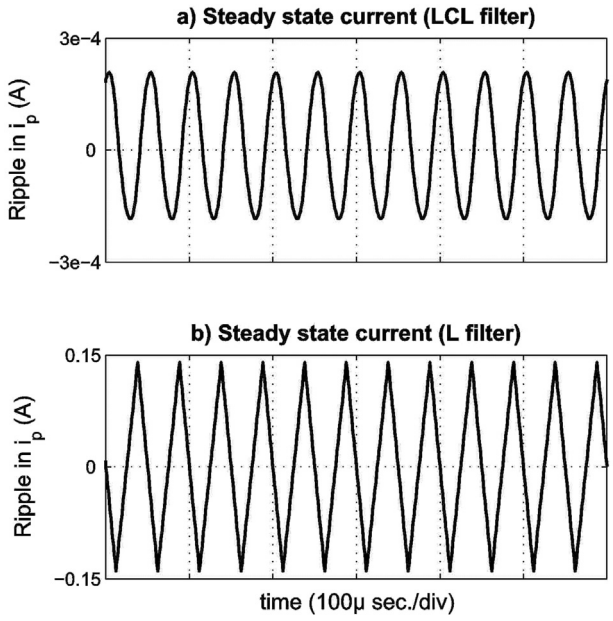

Fig. 9. Simulation Result: ripple of the drained current i_p. a) *LCL* case. b) *L* case.

overshoot can be adjusted to a desirable value by changing the position of the pole in the transfer function used to filter i_p^*. In Fig. 4b, the time response obtained by using a filter whose transfer function is $F_2 = 1/(-s/2s_1 + 1)$ is shown (see dashed line). In this case, the pole is farther than the pole used in F_1.

In order to test the robustness of the closed-loop system, L_1 and C value were varied ±25%, whereas the controller parameters computed with $L_1 = L_1^{nom}$, and $C = C^{nom}$ were kept constants. In such a case, the maximum real part of closed-loop poles was calculated $\sigma_{max} = max[\Re(p_{i=1,\ldots,8})]$ (where $\Re$ stands for real part and p_i are the roots of $H_{CL}(s) = 0$). Fig. 5 shows these values, normalized by ω_0. Note that for $C = C^{nom}$ (solid line), when L_1 differs from L_1^{nom}, σ_{max} differs from -0.7ω_0 closing to the real axis. However, the system stability is maintained when L_1 varies ±25% with respect to its nominal value. In presence of these variations, the stability is maintained when C varies ±25% with respect to its nominal value, such as illustrated in Fig. 5 (see dashed line and dash-dotted line).

4. Simulation and experimental results

The controller analyzed in the previous section was simulated and implemented. The simulation diagram and the experimental set up are shown in Fig. 6 and Fig. 7, respectively.

In order to show the system behavior under the worst condition, when it is excited by using high frequency components, the reference i_p^* filter was not implemented.

The following values were set: sampling time $T_s = 10^{-4}$ s, processing time delay $T_s/2$, PWM frequency = 20 KHz, $v_{dc} = 100$ V and $v_p = 50$ V. The ideal switches were assumed in simulations, working with a dead-time equal to 1 µs. The duty cycle d of the upper switch was chosen equal to $d = v_i^*/v_{dc}$, where v_{dc} was assumed a measured value. The digital controller was implemented by discretizing the transfer function $G(s)/s$ ($G(s)$ in series with the integrator) by using a first-order hold in the input (triangular approximation [40]). Fig. 8a (thick trace) shows the simulated output time response when the reference is a step signal. The time response is underdamped and it presents a peak such as was predicted (see Fig. 4b). Also, it presents a superimposed oscillation that is extinguished after a couple of cycles, oscillation that does not appear in Fig. 4b. This difference exists because the delay was approximated (see (2)), in order to obtain the time response illustrated in Fig. 4b, and an actual delay was utilized in obtaining the response of Fig. 8a.

In order to verify the influence of the equivalent series resistance of the components (ESR) -i.e. no ideal components-in the time response, an ESR in series with L_1, an ESR in series with L_2 and an ESR in series with C were added. The values of these components were 0.22 Ω, 0.136 Ω and 0.23 Ω, respectively. Simulation results are shown in Fig. 8b (thin trace). It can be seen that the initial peak value is reduced due to the ESR influence. It is the expected result since the ESR inclusion increases the damping. The analysis does not include parasitics components, since in this way the worst case design is achieved [21].

For comparison reasons, in Fig. 8b, the response obtained by using an L filter, $L = L_1 + L_2$, controlled by a PI controller was drawn.

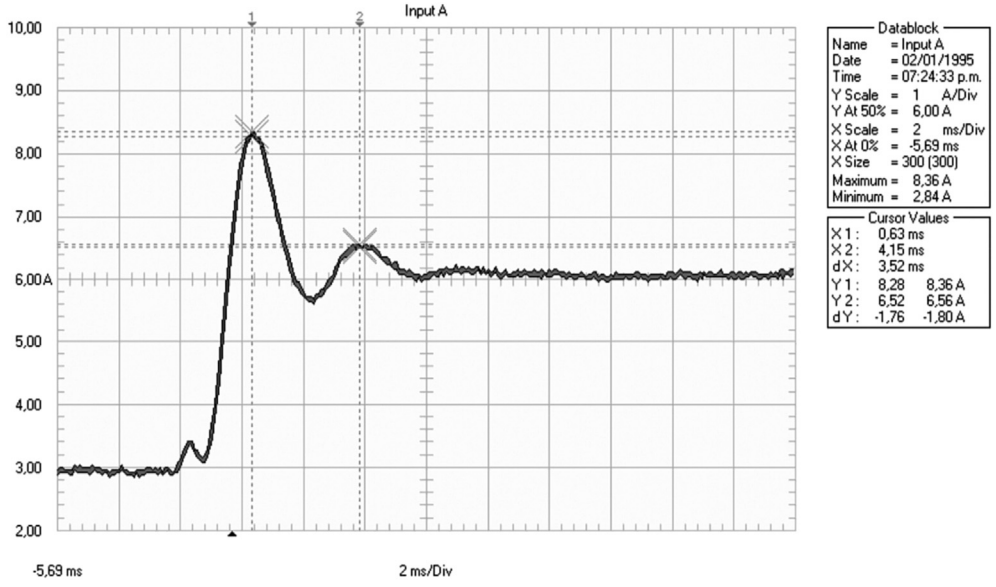

Fig. 10. Experimental results. Injected current i_p.

The PI gains were calculated for locating a conjugate complex pair of poles at $0.38\omega_0(-1 \pm j)$, such that a similar settling time was obtained. Fig. 9 shows the ripple in the drained current i_p for each case. It can be seen that the ripple value obtained with the *LCL* filter is much lower than the ripple value obtained with the *L* filter.

In order to verify the results obtained in the simulation, a prototype was implemented using $L_1 = 2.35$ mH (ESR 0.22 Ω); $L_2 = 2.09$ mH (ESR 0.136 Ω), $C = 91$ μF (ESR 0.23 Ω), and by using the same controller. Fig. 10 shows the obtained response, which is consistent with the results shown in Fig. 8a.

5. Conclusions

A current controller for a low resonance *LCL* filter used in dc–dc boost converters was introduced. A PI controller was modified including a linear network in series with the PI integral term. The inclusion of this linear network constitutes the main feature of the proposed controller. This network allows to arbitrarily place the closed-loop poles of the whole system. The proposed controller allows to guarantee the *LCL* topology stability increasing the computational burden a bit. By using the *LCL* filter, the ripple of the current drained to the source is reduced a lot by keeping the needed value of the inductance. It must be remarked that one current measurement is only needed for the implementation of the proposed controller.

Acknowledgments

This work was supported by Universidad Nacional del Sur, CONICET and ANPCyT, Argentina.

References

[1] Caro SD, Testa A, Triolo D, Cacciato M, Consoli A. Low input current ripple converters for fuel cell power units. In: Power Electronics and Applications, 2005 European Conference; 2005. p. 10.
[2] Benavides N, Chapman P. Modeling the effect of voltage ripple on the power output of photovoltaic modules. Industrial Electron IEEE Trans 2008;55(7):2638–43.
[3] Leu C-S, Nha QT. A half-bridge converter with input current ripple reduction for dc distribution systems. Power Electron IEEE Trans April 2013;28:1756–63.
[4] Barote L, Marinescu C. Software method for harmonic content evaluation of grid connected converters from distributed power generation systems. Energy 2014;66:401–12.
[5] Singh G. Solar power generation by pv (photovoltaic) technology: a review. Energy 2013;53:1–13.
[6] Liou W-R, Lacorte WB, Caberos AB, Yeh M-L, Lin J-C, Lin S-C, et al. A programmable controller ic for dc/dc converter and power factor correction applications. Industrial Inform IEEE Trans Nov 2013;9:2105–13.
[7] Jiang S, Cao D, Li Y, Peng FZ. Grid-connected boost-half-bridge photovoltaic microinverter system using repetitive current control and maximum power point tracking. Power Electron IEEE Trans Nov. 2012;27:4711–22.
[8] York B, Yu W, Lai J-S. Hybrid-frequency modulation for pwm-integrated resonant converters. Power Electron IEEE Trans Feb. 2013;28:985–94.
[9] York B, Yu W, Lai J-S. An integrated boost resonant converter for photovoltaic applications. Power Electron IEEE Trans March 2013;28:1199–207.
[10] Changwoo Y, Kim J, Choi S. Multiphase dc dc converters using a boost-half-bridge cell for high-voltage and high-power applications. Power Electron IEEE Trans Feb. 2011;26:381–8.
[11] Mirzaei A, Jusoh A, Salam Z. Design and implementation of high efficiency non-isolated bidirectional zero voltage transition pulse width modulated dc-dc converters. Energy 2012;47:358–69.
[12] Choi S, Agelidis V, Yang J, Coutellier D, Marabeas P. Analysis, design and experimental results of a floating-output interleaved-input boost-derived dc-dc high-gain transformer-less converter. Power Electron IET January 2013;4:168–80.
[13] Hegazy O, Van Mierlo J, Lataire P. Analysis, modeling, and implementation of a multidevice interleaved dc/dc converter for fuel cell hybrid electric vehicles. Power Electron IEEE Trans Nov. 2012;27:4445–58.
[14] Jung D-Y, Ji Y-H, Park S-H, Jung Y-C, Won C-Y. Interleaved soft-switching boost converter for photovoltaic power-generation system. Power Electron IEEE Trans April 2011;26:1137–45.
[15] Ho C-M, Breuninger H, Pettersson S, Escobar G, Canales F. A comparative performance study of an interleaved boost converter using commercial si and sic diodes for pv applications. Power Electron IEEE Trans 2013;28(1):289–99.
[16] Pena-Alzola R, Liserre M, Blaabjerg F, Sebastian R, Dannehl J, Fuchs F. Systematic design of the lead-lag network method for active damping in LCL-filter based three phase converters. Industrial Inform IEEE Trans Feb 2014;10:43–52.
[17] Yin J, Duan S, Liu B. Stability analysis of grid-connected inverter with LCL filter adopting a digital single-loop controller with inherent damping characteristic. Industrial Inform IEEE Trans 2013;9(2):1104–12.
[18] Balasubramanian A, John V. Analysis and design of split-capacitor resistive inductive passive damping for LCL filters in grid-connected inverters. Power Electron IET September 2013;6:1822–32.
[19] Mukherjee N, De D. Analysis and improvement of performance in LCL filter-based pwm rectifier/inverter application using hybrid damping approach. Power Electron IET February 2013;6:309–25.
[20] Xu J, Xie S, Tang T. Evaluations of current control in weak grid case for grid-connected LCL-filtered inverter. Power Electron IET February 2013 10;6:227–34.
[21] Liserre M, Blaabjerg F, Hansen S. Design and control of an LCL-filter-based three-phase active rectifier. Industry Appl IEEE Trans 2005;41(5):1281–91.
[22] Bierhoff M, Fuchs F. Active damping for three-phase pwm rectifiers with high-order line-side filters. Industrial Electron IEEE Trans 2009;56(2):371–9.
[23] Dannehl J, Fuchs F, Hansen S, Thøgersen P. Investigation of active damping approaches for PI-based current control of grid-connected pulse width modulation converters with LCL filters. Industry Appl IEEE Trans 2010;46(4):1509–17.
[24] Tang Y, Loh PC, Wang P, Choo FH, Gao F, Blaabjerg F. Generalized design of high performance shunt active power filter with output LCL filter. Industrial Electron IEEE Trans 2012;59(3):1443–52.
[25] Pe¯na-Alzola R, Liserre M, Blaabjerg F, Sebastián R, Dannehl J, Fuchs F. Analysis of the passive damping losses in LCL-filter-based grid converters. Power Electron IEEE Trans 2013;28(6):2642–6.
[26] Park S-Y, Chen C-L, Lai J-S, Moon S-R. Admittance compensation in current loop control for a grid-tie LCL fuel cell inverter. Power Electron IEEE Trans 2008;23(4):1716–23.
[27] Liu F, Zhou Y, Duan S, Yin J, Liu B, Liu F. Parameter design of a two-current-loop controller used in a grid-connected inverter system with LCL filter. Industrial Electron IEEE Trans 2009;56(11):4483–91.
[28] Tang Y, Loh PC, Wang P, Choo FH, Gao F. Exploring inherent damping characteristic of LCL-filters for three-phase grid-connected voltage source inverters. Power Electron IEEE Trans 2012;27(3):1433–43.
[29] Mohamed Y-R, A-Rahman M, Seethapathy R. Robust line-voltage sensorless control and synchronization of LCL -filtered distributed generation inverters for high power quality grid connection. Power Electron IEEE Trans 2012;27(1):87–98.
[30] Malinowski M, Bernet S. A simple voltage sensorless active damping scheme for three-phase pwm converters with an LCL filter. Industrial Electron IEEE Trans 2008;55(4):1876–80.
[31] Liserre M, Dell'Aquila A, Blaabjerg F. Stability improvements of an LCL-filter based three-phase active rectifier. In: PESC 02, vol. 3; 2002. p. 1195–201.
[32] Liserre M, Aquila A, Blaabjerg F. Genetic algorithm-based design of the active damping for an LCL-filter three-phase active rectifier. Power Electron IEEE Trans 2004;19(1):76–86.
[33] Dannehl J, Liserre M, Fuchs F. Filter-based active damping of voltage source converters with LCL filter. Industrial Electron IEEE Trans 2011;58(8):3623–33.
[34] Wu E, Lehn P. Digital current control of a voltage source converter with active damping of LCL resonance. Power Electron IEEE Trans 2006;21(5):1364–73.
[35] Bao X, Zhuo F, Tian Y, Tan P. Simplified feedback linearization control of three-phase photovoltaic inverter with an LCL filter. Power Electron IEEE Trans 2013;28(6):2739–52.
[36] Fantino R, Busada C, Solsona J. Controlador PI modificado para un convertidor boost bidireccional con filtro LCL en la entrada. In: Biennial Congress of Argentina (ARGENCON), 2014 IEEE; June 2014. p. 61–6.
[37] Blasko V, Kaura V. A novel control to actively damp resonance in input LC filter of a three-phase voltage source converter. Industry Appl IEEE Trans 1997;33(2):542–50.
[38] Blasko V, Kaura V. A new mathematical model and control of a three-phase ac-dc voltage source converter. Power Electron IEEE Trans Jan 1997;12:116–23.
[39] Parker S, McGrath B, Holmes D. Regions of active damping control for LCL filters. Industry Appl IEEE Trans Jan 2014;50:424–32.
[40] Franklin G, Powell J, Workman M. Digital control of dynamic systems. 2nd ed. Addison-Wesley; 1990.